ACS MATERIALS Au
AN OPEN ACCESS JOURNAL OF THE AMERICAN CHEMICAL SOCIETY

pubs.acs.org/materialsau

Article

Engineering Spherically Super-Structured Polyamides for the Sustainable Water Remediation

Rajan Kumar, Elizabathe Davis, Pradyumna Mazumdar, Diganta Choudhury, and Raja Shunmugam*

Cite This: *ACS Mater. Au* 2022, 2, 117−123

Read Online

ACCESS | Metrics & More | Article Recommendations | Supporting Information

ABSTRACT: Unlike metal-ornamented hybrid material and linear polymers, we invoked the growth of a biodegradable superstructured cross-linked polyamide-ester material. The material is thermally stable. The thiol-alkene photoclicked material acted as an efficient water remediator. The material efficiently monitored amphiphilic dyes like rhodamine B (RHB), methylene blue (MB), and chronic mercuric ions in water. The adsorption kinetics revealed the material could adsorb >95% dyes within 24 h. The RHB-functionalized polymer could sense mercuric ions too. The Density functional theory (DFT) calculation shows a chelated mercury complex with thioether in the polymer, **Poly-Am-RhAll**, to form a comparatively more stable complex.

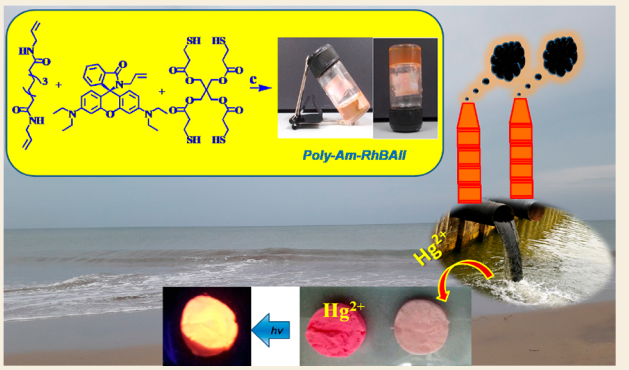

KEYWORDS: *amide, thiol-alkene photoclick reaction, hydrothiolation, dye, adsorption, mercury, sensor, DFT calculation*

1. INTRODUCTION

Contamination in nature is a combination of both natural and anthropogenic factors. Both organic and inorganic wastes influence the body's metabolism, giving rise to either curable or noncurable diseases. Organic dyes[1−7] and chronic mercury ion (Hg^{2+}) released from industries are water-polluting constituents. The toxicity from textile dyes and pigments can cause nausea, hypertension, cancer, etc. To overcome such effects, researchers have invoked several methods of engineering material for removal and sensing of wastes. Ali et al. utilized γ-alumina for the adsorption of methylene blue.[1] Qasem et al. reported a copper oxide nanoparticle as an efficient nanocatalyst for the catalytic reduction process of methylene blue.[2] Sar et al. reported glutamic-acid-derived cross-linked polymer that showed high efficiency to dye adsorption for crystal violet and malachite green.[3] Mohammadi et al. reported activated carbon to be utilized for adsorption of rhodamine B.[4] Bhattacharya et al. reported adsorption analysis for rhodamine B with a switch in the chain length of polyethylene glycol into a cross-linked network.[5] Kumar et al. reported biodegradable cross-linked polyesters for the removal of amphiphilic dyes from water.[6,7]

Apart from organic dyes, the intake of soft mercury ions can cause severe disorder in the body's metabolism. Anything above 2 ng/(L day) can be lethal to life. Exposure to mercuric ion or organo alkyl mercurates $Hg(R)^{+}$ causes premature birth. Several complexities arise in the central nervous system (CNS), liver, kidney, etc. Minamata disease, a neurological disorder, occurs because of methyl mercury. This highly toxic methyl mercury bioaccumulated in fish results in mercury poisoning when consumed by the local population. Therefore, monitoring the presence of mercuric ions in water bodies is essential. For monitoring its presence in water bodies, several molecular models have been introduced.[8−27] Aguado et al. reported thiol-functionalized SBA-15 mesoporous silicas showing efficient adsorption of inorganic mercuric ions.[9] Qasem et al. reported that F108-stabilized copper oxide shows high selectivity and sensitivity for determination of inorganic mercuric ion using resonance Rayleigh scattering methodology.[12] Shu et al. reported a naphthalene derivative as a probe that can show sensitivity to detection of both organic and inorganic mercury ions assisted by H_2O_2.[14] Voutsadaki et al. reported a water-soluble coumarin-based highly selective fluorescent probe for mercuric ion.[22] Zhang et al. engineered the surface of natural cellulose to show both the colorimetric detection and adsorption of mercuric ions.[27] However, most materials cannot be utilized in day-to-day life because of their specific drawbacks. In most cases, the adopted approaches require tedious synthetic processes in addition to being toxic and requiring heavy investment. The present material models implemented for monitoring the mercuric ion are active in either a semiaqueous or aqueous phase. So toward preventive

Received: September 1, 2021
Revised: October 19, 2021
Accepted: October 20, 2021
Published: November 8, 2021

https://doi.org/10.1021/acsmaterialsau.1c00042
ACS Mater. Au 2022, 2, 117−123

Scheme 1. Synthetic Schemes for Monomer AmAll, RhBAll, and Polymer Poly-Am-RhBAll[a]

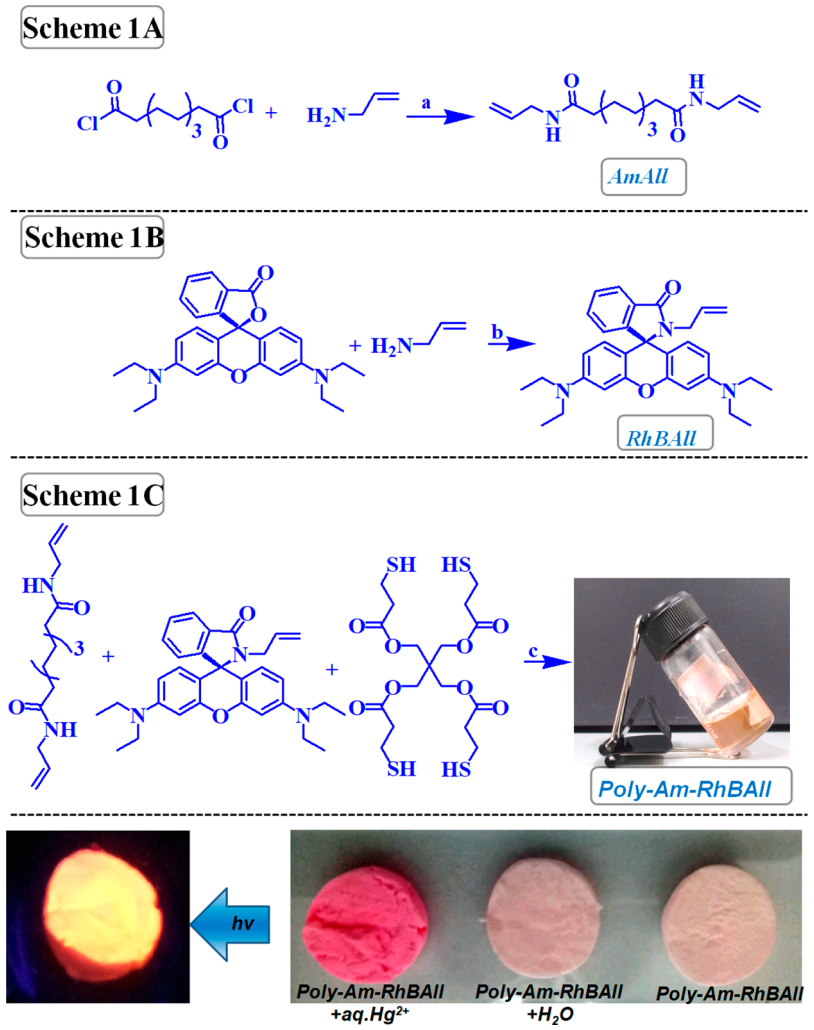

[a]Pictorial data for (i) washed and dried gel, (ii) treated gel in chronic mercuric solution, (iii) dried mercury treated polymer, and (iv) fluorescence for mercury treated **Poly-Am-RhBAll** (left to right). Reaction conditions: a = 5 °C-rt, DMSO, 24 h; b = ethanol, reflux, 24 h; c = 2-hydroxy-4′-(2-hydroxyethoxy)-2-methylpropiophenone, *hv*, DMSO, 3 h.

measurement, we need to develop a nontedious and cost-effective process for the growth of functional materials. Such material can be deployed for the effective removal of dyes and soft mercury ions along with colorimetric detection of mercuric ions.

In the context of the growth of such functional materials, we aim to engineer a water-immiscible biodegradable polymeric material that can remove dyes with ease. Therefore, we adopted a photoclick reaction[5−7,28,29] technique to grow a water-immiscible polymer to prevent solvent-related issues while monitoring wastes in water.

2. EXPERIMENTAL SECTION

2.1. Materials

Sebacoyl chloride, allylamine, rhodamine B, mercuric chloride, cadmium chloride, 2-Hydroxy-4′-(2-hydroxyethoxy)-2-methylpropiophenone, and penterthritoltetrakis (3-mercaptopropionate) were supplied by Aldrich. Solvents chloroform ($CHCl_3$), dimethyl sulfoxide (DMSO), and ethanol were used as provided.

2.2. Methods

Nuclear Magnetic Resonance (NMR) Spectroscopy. NMR spectroscopy was carried out on a Bruker 500 MHz using $CDCl_3$ and DMSO-d_6 as a solvent. NMR spectra of solutions in $CDCl_3$ and DMSO-d_6 were calibrated to tetramethylsilane as internal standard (δH 0.00).

Electrospray Ionization Mass Spectrometry (ESI MS). Electrospray ionization mass spectrometry (ESI MS) analysis was performed using a Bruker Maxis impact spectrometer.

CHN Analyzer. The elemental analysis was done using a PerkinElmer 2400 series II CHNS/O elemental analyzer.

Thermogravimetric Analysis (TGA). TGA was carried out using a PerkinElmer thermogravimetric analyzer at a heating rate of 10 °C/min. The temperature range was 50−600 °C.

Field-Emission Scanning Electron Microscopy (FE SEM). Field-emission scanning electron microscope (FE SEM), energy-dispersive X-ray (EDX), and mapping analyses were performed on a Zeiss microscope and a SUPRA 55VP field-emission scanning electron microscope.

Attenuated Total Reflectance Fourier Transform Infrared (ATR FTIR). ATR-FTIR spectroscopy analysis was performed on a Bruker ALPHA (Platinum ATR).

Transmission Electron Cryo-microscopy. Cryo TEM imaging was done using a transmission electron microscope (TEM, JEM2100F) at 120 kV. The emitter source used was LAB6. The camera used to capture images was a GATAN CCD camera. The sample for Cryo TEM was prepared on a GATAN Cryoplunger-3(Cp-3) using N_2 gas, liquid N_2, and liquid ethane with the

https://doi.org/10.1021/acsmaterialsau.1c00042
ACS Mater. Au 2022, 2, 117−123

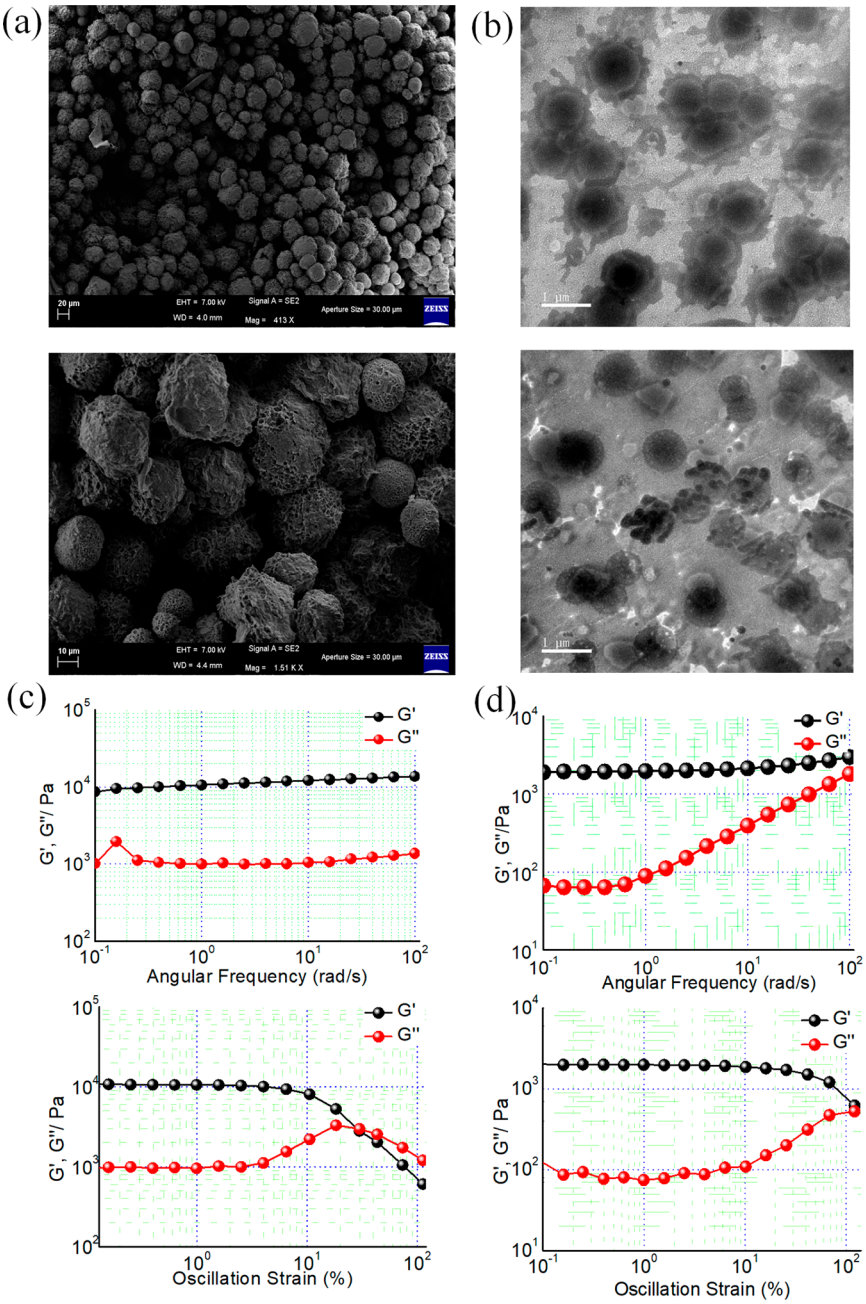

Figure 1. (a) FE SEM (scale bars 20 μm for top and 10 μm for bottom). (b) Cryo-TEM images for **Poly-Am-All** (1 μm). Rheometric analysis for polymers (c) **Poly-Am-All** and (d) **Poly-Am-RhBAll**.

temperature maintained at −160 °C. The temperature was monitored up to −180 °C on a Gatan model no. 1905.C1D00. The TEM grid holder was preserved in a GATAN turbo pumping station (model 655) to avoid moisture. The pumping pressure was monitored in the range of 1×10^{-3} to 1×10^{-4} Pa.

Rheometer. Dynamic Storage modulus (G') and loss modulus (G'') versus angular frequency/oscillation strain were recorded on a TA-ARG2 rheometer (using a steel parallel plate with a 60 mm diameter) connected to a Peltier circulator thermo cube with a Peltier plate.

Ultraviolet Visible (UV Vis) Spectroscopy. UV−vis absorption measurements were carried out on PerkinElmer Lambda-35 UV−vis spectrometer. Solid-state UV−visible absorption measurements were carried out on Jasco V-670, a UV−vis spectrometer.

Fluorescence Spectroscopy. Solid-state fluorescence emission and fluorescence lifetime decay were carried out on a fluorescence spectrometer (Horiba Jobin Yvon, Fluoromax- 3, Xe-150 W, 250−900 nm) at 298 K.

2.3. Synthetic Procedures

Synthesis of Monomer AmAll. Sebacoyl chloride (4.18 mmol) dissolved in dry DMSO (50 mL) was taken in a 250 mL round-bottom flask with a magnetic stirrer. The temperature was maintained at 5 °C. Allyl amine (18.18 mmol) was added dropwise. The reaction mixture under N_2 gas was stirred for 24 h. The product precipitated in distilled water was dried using a Buchner funnel. Yield: 93%. ^{1}H NMR (DMSO-d_6, Bruker-500 MHz) δ (in ppm): 7.87(s, 2H), 5.7(m, 2H), 5.0(m, 4H), 2.0(m, 4H), 1.4(m, 4H), 1.18(m, 12H). ^{13}C NMR (DMSO-d_6, Bruker-500 MHz) δ (in ppm): 172.5, 136.0, 115.4, 41.2, 35.8, 29.19, 29.16, 25.8. Calculated for $C_{16}H_{28}N_2O_2$: C 68.53, H 10.06, N 9.99; found: C 67.72, H 10.42, N 9.9. ATR FTIR stretch (in cm^{-1}): 3257, 3033, 2881, 2814, 1610, 1516, 1449.

https://doi.org/10.1021/acsmaterialsau.1c00042
ACS Mater. Au 2022, 2, 117−123

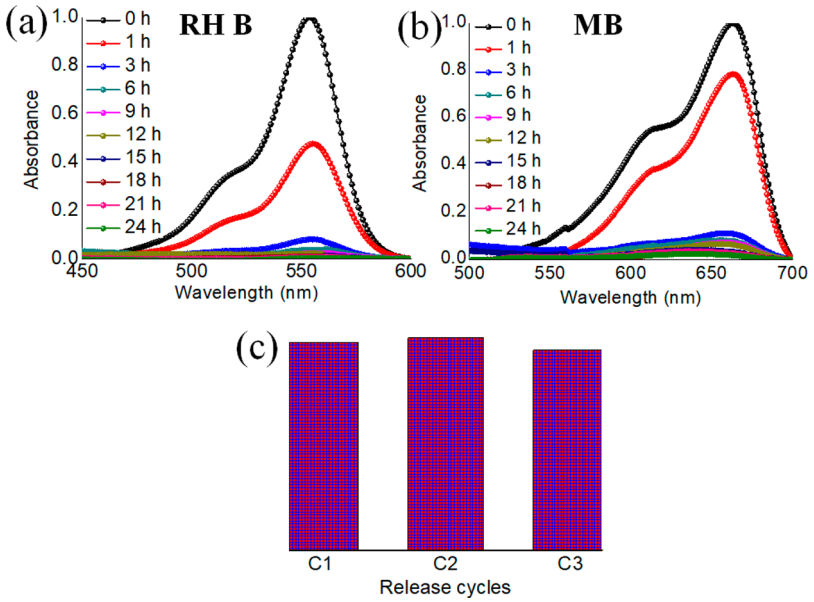

Figure 2. (a, b) Kinetics for removing rhodamine B (RHB) and methylene blue (MB) in the presence of **Poly-Am-All**. (c) Recycling of **Poly-Am-All** for RHB release over cycles C1−C3.

Synthesis of RhBAll. Rhodamine B (2.26 mmol) in ethanol (100 mL) was taken in a 250 mL round-bottom flask equipped with magnetic stirrer. Allyl amine (3.39 mmol) was added dropwise. The reaction mixture was refluxed for 24 h. The product precipitated in distilled water was washed and dried using Buchner funnel. Yield: 90%. ^{1}H NMR ($CDCl_3$, Bruker-500 MHz) δ (in ppm): 7.8(m, 1H), 7.4(m, 2H), 7.0(m, 1H), 6.4(m, 2H), 6.38(m, 2H), 6.33(m, 2H), 6.24(s, 2H), 6.22(m, 2H), 5.3(m, 1H), 4.8−4.7(m, 2H), 3.7(m, 2H), 3.3(m, 8H), 1.12(m, 12H). ^{13}C NMR ($CDCl_3$, Bruker-500 MHz) δ (in ppm): 167.52, 153.46, 133.4, 132.3, 131.38, 129.0, 127.8, 123.76, 116.33, 108.0, 105.9, 97.7, 64.7, 44.3, 42.5, 12.54. HRMS (ESI) m/z: $[M + H]^+$ calculated for $C_{31}H_{36}N_3O_2$, 482.3; found, 482.2803. Anal. Calculated for $C_{31}H_{36}N_3O_2$: C 77.31, H 7.32, N 8.72; found: C 77.29, H 7.18, N 8.96. ATR FTIR stretch (in cm^{-1}): 2929, 2891, 2838, 1663, 1595, 1494.

Synthesis of Polymer Poly-Am-All. AmAll (0.71 mmol) and penterthritoltetrakis (3-mercaptopropionate) **4SH** (0.35 mmol) were introduced into a 15 mL vial followed by the addition of a catalytic amount of initiator 2-hydroxy-4′-(2-hydroxyethoxy)-2-methylpropiophenone. Synthetic DMSO (5 mL) was added. The system was then purged with N_2 gas for 10 min via a Schlenk tube. The reaction mixture was irradiated for 3 h under UV light at a wavelength of 365 nm. The crude solid polymer **Poly-Am-All** was washed in DMSO (5 mL) repeatedly and then washed in chloroform and dried. ^{1}H NMR (DMSO-d_6, Bruker-500 MHz) confirmed the formation of **Poly-Am-All**. Yield: 93%. ATR FTIR stretch (in cm^{-1}): 3267, 2878, 2819, 1712, 1615, 1523.

Synthesis of Polymer Poly-Am-RhBAll. AmAll (0.77 mmol), **RhBAll** (0.081 mmol), andpenterthritoltetrakis (3-mercaptopropionate) **4SH** (0.409 mmol) were introduced into 15 mL vial followed by the addition of a catalytic amount of initiator -2-Hydroxy-4′-(2-hydroxyethoxy)-2-methylpropiophenone. Synthetic DMSO (5 mL) was added to the reaction mixture. The system was then purged with N_2 gas for 10 min via a Schlenk tube. The reaction mixture was then irradiated for 3 h under UV light at wavelength 365 nm. The crude solid polymer was washed in DMSO repeatedly, followed by washing in chloroform and drying. ^{1}H NMR (DMSO-d_6, Bruker-500 MHz) confirmed the formation of **Poly-Am-RhBAll**. Yield: 92%. ATR FTIR stretch (in cm^{-1}): 3261, 3038, 2881, 2818, 1704, 1615, 1511, 1444.

3. RESULTS AND DISCUSSIONS

To overcome the limitations, we came up with the thiol-alkene photoclick polymerization reaction to grow 3D-polymer **Poly-Am-All**, which shows dual response to water remediation. **Poly-Am-RhBAll** was functionalized with allyl functional monomer **RhBAll** to monitor mercury ions via sensing. The polymer **Poly-Am-RhBAll** synthesized is shown in Scheme 1. The ^{1}H NMR, ^{13}C NMR, ESI MS, UV−vis, and CHN analysis confirmed the formation of monomers **AmAll** and **RhBAll** (Figures S1−S4 and S7−S9). UV−vis analysis for monomer **RhBAll** showed no absorbance maximum at ∼550 nm. This confirmed the presence of a closed spirolactone ring.

Moreover, the ^{13}C NMR spectrum for the **RhBAll** showed C_k carbon (Figure S2), which supported forming a closed spirolactone ring. The ATR FTIR confirmed the thiol (SH) functionality consumed during the hydrothiolation to form the polymers **Poly-Am-All** and **Poly-Am-RhBAll**. The thermal properties of **Poly-Am-All** revealed thermal stability up to around 300 °C (Figure S10). ^{1}H NMR for **Poly-Am-RhBAll** revealed the presence of aromatic signals (Figure S6). This confirmed the **RhBAll** to have linked covalently during the formation of **Poly-Am-RhBAll** via hydrothiolation. Thus, both **Poly-Am-All** and **Poly-Am-RhBAll** are functional heterogeneous material, which remains immiscible in an aqueous environment.

Further, the FESEM and Cryo TEM morphology of **Poly-Am-All** is showed in Figure 1a, b. The morphology reflects the formation of super spherical structures. Such structures are assumed to increase the surface exposure to the aqueous environment.

The viscoelastic property for the polymers was analyzed using a rheometer. **Poly-Am-All** and **Poly-Am-RhBAll** were mounted onto the rheometer, and the analysis was monitored at constant frequency sweep and amplitude sweep. Both **Poly-Am-All** and **Poly-Am-RhBAll** (Figure 1c, d) exhibited elastic modulus G' greater than viscous modulus G''. Further, the curves revealed the material to have a damping factor tan δ $(G''/G') < 1$, which means the material retains both elastic and viscous properties. Therefore, the material is viscoelastic.

The polymer **Poly-Am-All** was tested for adsorption of colorants such as rhodamine B (RHB) and methylene blue (MB) in its application. On analysis, we found MB could be

https://doi.org/10.1021/acsmaterialsau.1c00042
ACS Mater. Au 2022, 2, 117−123

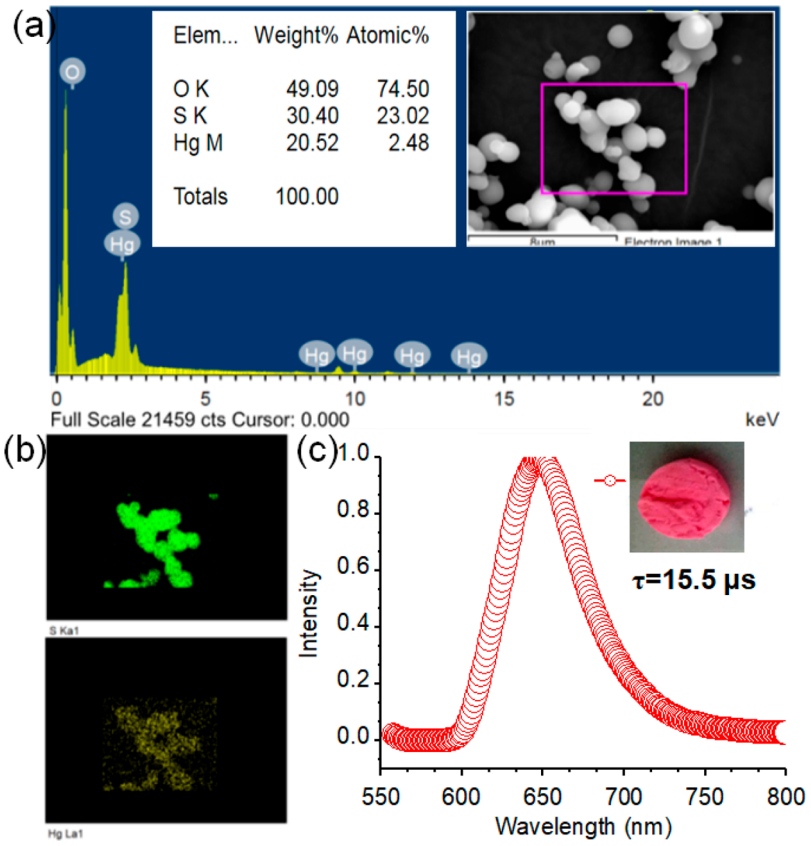

Figure 3. (a) EDX, (b) mapping for **Poly-Am-All** with treated mercuric ion, (c) fluorescence curve for **Poly-Am-RhBAll** with treated mercuric ion.

removed with 10 mg of **Poly-Am-All**, whereas 20 mg was sufficient to remove RHB over a time duration of 24 h. The dye concentration considered for analysis was fixed at 0.01 mM/mL. The kinetics study for the adsorption of dyes by **Poly-Am-All** revealed that the polymeric material could take up optimum dyes within the time interval of 24 h. The optimum uptake was found to be >95% within 24 h. The kinetics analysis for the removal of dyes is shown in Figure 2a, b. The release of dye RHB was significant in polar protic solvent methanol. The recycling of **Poly-Am-All** showed efficient release for RHB over cycles as observed in Figure 2c. Such dye released and recoveredis crucial from the aspect of sensing the waste present in water.

The polymer **Poly-Am-All** with thioether formed during hydrothiolation was tested for mercury removal too. The polymer was dipped in a 20 ppm mercury solution and dried. The mercury-treated dried polymer was analyzed via the EDX technique, shown in Figure 3a. The analysis revealed the mercury ion was adsorbed onto the **Poly-Am-All**. Moreover, the presence of sulfur confirmed that cross-linking via hydrothiolation took place. Mapping analysis shown in Figure 3b and Figure S11 parallelly supports the EDX analysis. The **Poly-Am-RhBAll** was tested for mercuric ion (Hg^{2+}) and compared with the cadmium (Cd^{2+}) ion. The polymer showed significant color change for mercuric ions. When the concentration of mercuric ion (Hg^{2+}) was in the range of 2−200 ppm with a constant volume of mercury solution (100 mL), **Poly-Am-RhBAll** showed an increase in intensity for the colorimetric response with an increase in concentration of the mercuric ion in solution. The light orange color changed to pink, intensifying at a higher parts per million value (Scheme 1). The solid-state UV−vis curve showed a distinct difference in absorbance before and after treatment with mercuric ions (Figure S12). A new absorbance band appears in the visible region where **Poly-Am-RhBAll** interacted with mercuric ions. This corresponds to the opening of the spirolactone ring.[19−21] The fluorometric analysis responded well. The fluorometric curve in Figure 3c showed a red-shifted emission. This corresponds to the **RhBAll** component being grafted in **Poly-Am-RhBAll**, in which the spirolactone ring opens while coming into contact with the mercuric ion. The significant soft−soft interaction of Hg^{2+} with thioether sulfur (S) is the prime cause for removing and sensing mercuric ions. The fluorescence lifetime for the mercury-treated **Poly-Am-RhBAll** was performed. The observation revealed the treated polymer to show a lifetime of 15.5 μs (Figure S13).

DFT was performed to understand the active mode of interactions at the active site in **Poly-Am-RhBAll** with mercuric ions.[30−35] To understand the stability of complexes where mercury is chelating with and without sulfur S, we performed the DFT computational calculations using *Gaussian 09* software. To study sulfur's role, we introduced and computed three sets of complexes assigned as C-1, C-2, and C-3. All the structures were optimized using the SDD basis set for Hg and the 6-311G (d,p) basis set for other atoms. On calculation using *Gaussian 09*, we observed complexes C-2 (−696.5085935 kcal/mol) and C-3 (−691.6808115 kcal/mol) where sulfur S atoms involved in chelation with mercury form more stable complexes relative to complex C-1 (−633.5638372 kcal/mol). The computed complex structures are shown in Figure 4. This meant the sulfur S atoms' affinity for mercuric ions has an essential role in coloration to dark pink. These

https://doi.org/10.1021/acsmaterialsau.1c00042
ACS Mater. Au 2022, 2, 117−123

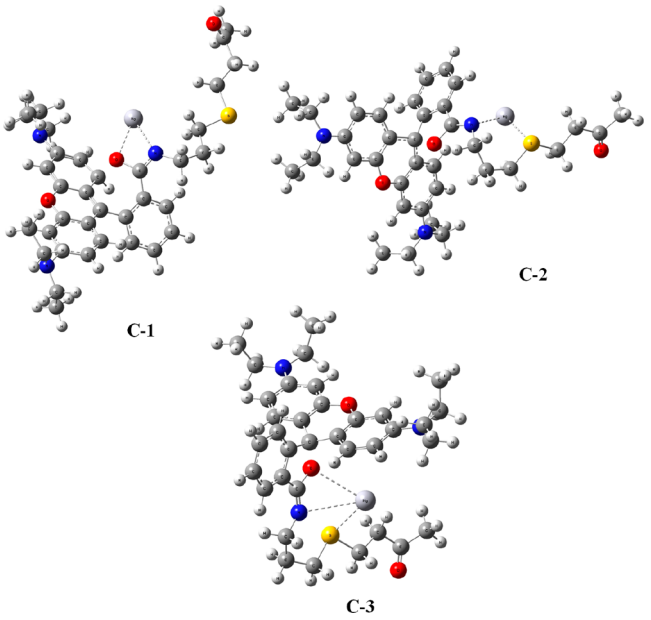

Figure 4. DFT optimized complex conformations. Note: red balls are oxygen (O), blue are nitrogen (N), and yellow are sulfur (S).

reveal mercury ions to accelerate the spirolactone ring opening during the complexation process

CONCLUSION

In summary, the efficiency of dual functional 3D photoclicked cross-linked polymers in the water remediation process was shown via monitoring the presence of dyes rhodamine B (RHB), methylene blue (MB), and mercuric ion (Hg^{2+}). The **RhBAll** polymer with such superstructures showed distinct colorimetric responses when treated with mercuric ions. Such a model system can identify the leakage of mercuric ions. This proves that polymers **Poly-Am-All** and **Poly-Am-RhBAll** can be ideal for retrieving water purity from toxic wastes. Moreover, the synthesis techniques to grow polyamide with no toxicity but high thermal stability with economic value can popularize its utility. The DFT studies supported the observation. Further, we plan to develop a commercial model using the reported polymer as a responsive material shortly.

ASSOCIATED CONTENT

Supporting Information

The Supporting Information is available free of charge at https://pubs.acs.org/doi/10.1021/acsmaterialsau.1c00042.

^{1}H NMR and ^{13}C NMR spectra of **RhBAll**, **AmAll**, **Poly-Am-All**, and **Poly-Am-RhBAll**; ESI MS and UV–vis for **RhBAll**; ATR-FTIR of **4SH**, **AmAll**, **RhBAll**, and **Poly-Am-RhBAll**; TGA of **Poly-Am-All**; mapping analysis of **Poly-Am-All** with Hg(II); solid-state UV–vis of **Poly-Am-RhBAll** without and with Hg(II); fluorescence lifetime curve of **Poly-Am-RhBAll** with Hg(II) (PDF)

AUTHOR INFORMATION

Corresponding Author

Raja Shunmugam − *Polymer Research Centre (PRC), Centre for Advanced Functional Materials (CAFM), Department of Chemical Sciences, Indian Institute of Science Education and Research Kolkata (IISER K), Mohanpur 741246 West Bengal, India;* orcid.org/0000-0002-0221-127X; Email: sraja@iiserkol.ac.in

Authors

Rajan Kumar − *Polymer Research Centre (PRC), Centre for Advanced Functional Materials (CAFM), Department of Chemical Sciences, Indian Institute of Science Education and Research Kolkata (IISER K), Mohanpur 741246 West Bengal, India; Department of Chemistry, Royal School of Applied and Pure Sciences (RSAPS), The Assam Royal Global University, Guwahati 781035 Assam, India*

Elizabathe Davis − *Polymer Research Centre (PRC), Centre for Advanced Functional Materials (CAFM), Department of Chemical Sciences, Indian Institute of Science Education and Research Kolkata (IISER K), Mohanpur 741246 West Bengal, India*

Pradyumna Mazumdar − *Department of Chemistry, B. Borooah College, Guwahati 781007 Assam, India*

Diganta Choudhury − *Department of Chemistry, B. Borooah College, Guwahati 781007 Assam, India*

Complete contact information is available at: https://pubs.acs.org/10.1021/acsmaterialsau.1c00042

Notes

The authors declare no competing financial interest.

ACKNOWLEDGMENTS

R.K. thanks IISER Kolkata for the research fellowship. E.D. thanks DST Inspire for the scholarship. R.S. thanks DBT and DST for research projects. The authors thank K.S. for the FESEM analysis. Finally, the authors thank IISER-Kolkata for the infrastructure facility.

REFERENCES

(1) Ali, S.; Abbas, Y.; Zuhra, Z.; Butler, I. S. Synthesis of γ-alumina (Al_2O_3) nanoparticles and their potential for use as an adsorbent in the removal of methylene blue dye from industrial wastewater. *Nanoscale Adv.* **2019**, *1*, 213−218.

(2) Qasem, M.; El Kurdi, R.; Patra, D. Green Synthesis of Curcumin Conjugated CuO Nanoparticles for Catalytic Reduction of Methylene Blue. *Chemistry Select* **2020**, *5*, 1694−1704.

(3) Sar, P.; Roy, S. G.; De, P.; Ghosh, S. Synthesis of Glutamic Acid Derived Organogels and their Applications in Dye Removal from Aqueous Medium. *Macromol. Mater. Eng.* **2020**, *305*, 1900809.

(4) Mohammadi, M.; Hassani, A. J.; Mohamed, A. R.; Najafpour, G. D. Removal of Rhodamine B from Aqueous Solution Using Palm Shell-Based Activated Carbon: Adsorption and Kinetic Studies. *J. Chem. Eng. Data* **2010**, *55*, 5777−5785.

(5) Bhattacharya, S.; Shunmugam, R. Unraveling the Effect of PEG Chain Length on the Physical Properties and Toxicant Removal Capacities of Cross-Linked Network Synthesized by Thiol−Norbornene Photoclick Chemistry. *ACS Omega* **2020**, *5*, 2800−2810.

(6) Kumar, R.; Rajpoot, A.; Roy, A.; Shunmugam, R. Engineering biodegradable polymeric network for the efficient removal of organo-amphiphilic toxicants. *Polym. Adv. Technol.* **2020**, *31*, 957−966.

(7) Kumar, R.; Shunmugam, R. Unique Design of Porous Organic Framework Showing Efficiency toward Removal of Toxicants. *ACS Omega* **2017**, *2*, 4100−4107.

(8) Tracey, M. P.; Koide, K. Development of a Sustainable Enrichment Strategy for Quantification of Mercury Ions in Complex Samples at the Sub-Parts per Billion Level. *Ind. Eng. Chem. Res.* **2014**, *53*, 14565−14570.

(9) Aguado, J.; Arsuaga, J. M.; Arencibia, A. Adsorption of Aqueous Mercury(II) on Propylthiol-Functionalized Mesoporous Silica Obtained by Cocondensation. *Ind. Eng. Chem. Res.* **2005**, *44*, 3665−3671.
(10) Granite, E. J.; Pennline, H. W.; Hargis, R. A. Novel Sorbents for Mercury Removal from Flue Gas. *Ind. Eng. Chem. Res.* **2000**, *39*, 1020−1029.
(11) Gruss, A. F.; Rodriguez, R.; Mazyck, D. W. Mercury Oxidation by UV Irradiation: Effect of Contact Time, UV Wavelength, and Moisture Content. *Ind. Eng. Chem. Res.* **2017**, *56*, 6131−6135.
(12) Qasem, M.; El Kurdi, R.; Patra, D. F108 stabilized CuO nanoparticles for highly selective and sensitive determination of mercury using resonance Rayleigh scattering spectroscopy. *Anal. Methods* **2020**, *12*, 1631−1638.
(13) Ono, A.; Togashi, H. Highly Selective Oligonucleotide-Based Sensor for Mercury(II) in Aqueous Solutions. *Angew. Chem.* **2004**, *116*, 4400−4402.
(14) Shu, W.; Yan, L.; Liu, J.; Wang, Z.; Zhang, S.; Tang, C.; Liu, C.; Zhu, B.; Du, B. Highly Selective Fluorescent Probe for the Sensitive Detection of Inorganic and Organic Mercury Species Assisted by H_2O_2. *Ind. Eng. Chem. Res.* **2015**, *54*, 8056−8062.
(15) Lin, Z.-H.; Zhu, G.; Zhou, Y. S.; Yang, Y.; Bai, P.; Chen, J.; Wang, Z. L. A Self-Powered Triboelectric Nanosensor for Mercury Ion Detection. *Angew. Chem.* **2013**, *125*, 5169−5173.
(16) Huang, C.-C.; Yang, Z.; Lee, K.-H.; Chang, H.-T. Synthesis of Highly Fluorescent Gold Nanoparticles for Sensing Mercury(II). *Angew. Chem.* **2007**, *119*, 6948−6952.
(17) Ko, S.-K.; Yang, Y.-K.; Tae, J.; Shin, I. In Vivo Monitoring of Mercury Ions Using a Rhodamine-Based Molecular Probe. *J. Am. Chem. Soc.* **2006**, *128*, 14150−14155.
(18) Nolan, E. M.; Lippard, S. J. Turn-On and Ratiometric Mercury Sensing in Water with a Red-Emitting Probe. *J. Am. Chem. Soc.* **2007**, *129*, 5910−5918.
(19) Hazra, S.; Bodhak, C.; Chowdhury, S.; Sanyal, D.; Mandal, S.; Chattopadhyay, K.; Pramanik, A. A novel tryptamine-appended rhodamine-based chemosensor for selective detection of Hg^{2+} present in aqueous medium and its biological applications. *Anal. Bioanal. Chem.* **2019**, *411*, 1143−1157.
(20) Fang, Y.; Li, X.; Li, J.-Y.; Wang, G.-Y.; Zhou, Y.; Xu, N.-Z.; Hu, Y.; Yao, C. Thiooxo-Rhodamine B hydrazone derivatives bearing bithiophene group as fluorescent chemosensors for detecting mercury(II) in aqueous media and living HeLa cells. *Sens. Actuators, B* **2018**, *255*, 1182−1190.
(21) Samanta, T.; Shunmugam, R. Colorimetric and fluorometric probes for the optical detection of environmental Hg(ii) and As(iii) ions. *Mater. Adv.* **2021**, *2*, 64−95.
(22) Voutsadaki, S.; Tsikalas, G. K.; Klontzas, E.; Froudakis, G. E.; Katerinopoulos, H. E. turn-on" coumarin-based fluorescent sensor with high selectivity for mercury ions in aqueous media. *Chem. Commun.* **2010**, *46*, 3292−3294.
(23) Kong, R.-M.; Zhang, X.-B.; Zhang, L.-L.; Jin, X.-Y.; Huan, S.-Y.; Shen, G.-L.; Yu, R.-Q. An ultrasensitive electrochemical "turn-on" label-free biosensor for $Hg^{2+}$with AuNP-functionalized reporter DNA as a signal amplifier. *Chem. Commun.* **2009**, 5633−3635.
(24) Liu, B.; Tian, H. A selective fluorescent ratiometric chemodosimeter for mercury ion. *Chem. Commun.* **2005**, 3156−3158.
(25) Minami, T.; Sasaki, Y.; Minamiki, T.; Koutnik, P.; Anzenbacher, P.; Tokito, S. A mercury(II) ion sensor device based on an organic field effect transistor with an extended-gate modified by dipicolylamine. *Chem. Commun.* **2015**, *51*, 17666−17668.
(26) Choudhury, N.; Ruidas, B.; Mukhopadhyay, C. D.; De, P. Rhodamine-Appended Polymeric Probe: An Efficient Colorimetric and Fluorometric Sensing Platform for Hg^{2+} in Aqueous Medium and Living Cells. *ACS Appl. Polym. Mater.* **2020**, *2*, 5077−5085.
(27) Zhang, X.; Huang, J. Functional surface modification of natural cellulose substances for colorimetric detection and adsorption of Hg^{2+} in aqueous media. *Chem. Commun.* **2010**, *46*, 6042−6044.
(28) Tang, W.; Becker, M. L. Click" reactions: a versatile toolbox for the synthesis of peptide-conjugates. *Chem. Soc. Rev.* **2014**, *43*, 7013−7039.
(29) Lowe, A. B. Thiol-yne 'click'/coupling chemistry and recent applications in polymer and materials synthesis and modification. *Polymer* **2014**, *55*, 5517−5549.
(30) El-Azhary, A. A.; Suter, H. U. Comparison between Optimized Geometries and Vibrational Frequencies Calculated by the DFT Methods. *J. Phys. Chem.* **1996**, *100*, 15056−15063.
(31) Montero-Campillo, M. M.; Lamsabhi, A. M.; Mo, O.; Yanez, M. Alkyl mercury compounds: an assessment of DFT methods. *Theor. Chem. Acc.* **2013**, *132*, 1328.
(32) Rahman, S.; Zein, A.; Dawe, L. N.; Shamov, G.; Thordarson, P.; Georghiou, P. E. Supramolecular host−guest complexation of Lash's calix[4]azulene with tetraalkylammonium halides and tetrafluoroborate salts: binding and DFT computational studies. *RSC Adv.* **2015**, *5*, 54848−54852.
(33) de Azevedo, W. F., Jr.; Dias, R. Computational Methods for Calculation of Ligand-Binding Affinity, Current Drug Targets. *Curr. Drug Targets* **2008**, *9*, 1031−1039.
(34) Ducere, J.-M.; Goursot, A.; Berthomieu, D. Comparative Density Functional Theory Study of the Binding of Ligands to Cu^{+} and Cu^{2+}: Influence of the Coordination and Oxidation State. *J. Phys. Chem. A* **2005**, *109*, 400−408.
(35) Frisch, M. J.; Trucks, G. W.; Schlegel, H. B.; Scuseria, G. E.; Robb, M. A.; Cheeseman, J. R.; Scalmani, G.; et al. *Gaussian 09*, Revision C.01; Gaussian, Inc., Wallingford CT, 2010.

https://doi.org/10.1021/acsmaterialsau.1c00042
ACS Mater. Au 2022, 2, 117−123